Electronic supplementary information

Pressure-controlled microfluidic sub-picoliter ultramicro-volume syringes based on integrated micro-nanostructure arrays

Nianzuo Yu,[a] Yongshun Liu,*[,b] Shuli Wang,[c,d] Xiaoduo Tang,[a] Peng Ge,[a] Jingjie Nan,[a] Junhu Zhang,*[,a] and Bai Yang[a]

[a]State Key Laboratory of Supramolecular Structure and Materials, College of Chemistry, Jilin University, 130012, P. R. China

[b]State Key Laboratory of Applied Optics, Changchun Institute of Optics, Fine Mechanics and Physics (CIOMP), Chinese Academy of Sciences, 130033, P. R. China

[c]State Key Laboratory of Physical Chemistry of Solid Surface, College of Chemistry and Chemical Engineering, Xiamen University, Xiamen 361005, China.

[d]Collaborative Innovation Center of Chemistry for Energy Materials, Xiamen University, Xiamen 361005, China

*E-mail: zjh@jlu.edu.cn

Supporting Figure 1	Schematic illustration of cambered fluid front at the right edge of the MSNP
Supporting Figure 2	Schematic of the UVS
Supporting Table 1	Schematic of the UVS The dimension parameters of the UVS/G-UVS
Supporting Figure 3	The AFM, SEM images and repeatability measures of the MSNPs
Supporting Figure 4	The SEM images and repeatability measures of the microchannels
Supporting Figure 5	The ACA of the Si and PDMS surfaces
Supporting Figure 6	AFM images of the nanopillars with different etching time on the MSNP array surface
Supporting Figure 7	The duration and accuracy of the dispensing process as a function of the liquid pressure
Supporting Figure 8	Optical microscopy images of the UVSs with different measuring ranges
Supporting Figure 9	Accuracy, experimentally measured and theoretical bursting pressures of the UVS with different channel heights
Supporting Figure 10	Dispensing process, accuracy, experimentally measured and theoretical bursting pressures of the UVS with 50.0 pL division value
Supporting Figure 11	The ACA of the bonded Si surface
Supporting Figure 12	Dispensing process, accuracy, experimentally measured and theoretical bursting pressures of the 10-G-UVS
Supporting Figure 13	Accuracy, experimentally measured and theoretical bursting pressures of the 5-G-UVS
Supporting Figure 14	Dispensing process, accuracy, experimentally measured and theoretical bursting pressures of the 3-G-UVS
Supporting Figure 15	Dispensing process, manipulation pressures and accuracy of the 1-G-UVS
Supporting Figure 16	The capturing process of wide ST liquids
Supporting Figure 17	Accuracy of the dispensing process for wide ST liquids
Supporting Figure 18	Dispensing process, manipulation pressures of the synthetic process of Au nanoparticles
Supporting Figure 19	The diameter distribution and mean diameter of the Au nanoparticles
Supporting Figure 20	Dispensing process, manipulation pressures of the synthetic process of Au nanorods
Supporting Figure 21	The mean aspect ratio of the Au nanorods
Video S1	Capture of 6.00 nL water droplet by the UVS
Video S2	Capture of 6.00 nL 5% alcohol solution by the UVS

Experimental Section

Materials. Si and glass substrates were cleaned by immersion in piranha solution (7:3 concentrated H_2SO_4/30% H_2O_2) for 2 h at 140 °C to create a hydrophilic surface. A photoresist (BP218-45s positive photoresist) was purchased from Kempur Microelectronics. A Sylgard 184 elastomer base and a curing agent for PDMS were purchased from Dow Corning (Midland, MI). PFS, sodium borohydride (98%), and hexadecyltrimethyl ammonium bromide (99%) (CTAB) were purchased from Aldrich. Insulin, sodium fluorescein, rhodamine and anticoagulation newborn bovine blood was purchased from Solarbio, and the experimental blood sample was originated from the same bovine. Gold(III) chloride tetrahydrate ($HAuCl_4 \cdot 4H_2O$; ≥99.9%) was purchased from Sinopharm Chemical Reagent Co., Ltd. BSA, PVP (Mw=40000) and ascorbic acid (99%) were purchased from SIGMA. Silver nitrate (99.9% of Ag) was purchased from Strem Chemicals. Absolute ethanol and acetone were used as received. Milli-Q water (18.2 MΩ cm-1) was used in all experiments.

Device Fabrication. Fabrication of the hydrophobic silicon microstripe structures were performed as earlier, and the nanopillars on the microstripe surface were fabricated by a RIE etching method. Si molds for duplicating PDMS microchannels and glass microchannels were fabricated by conventional photolithography and inductively coupled plasma dry etching, and PDMS microchannels were prepared by soft lithography. The PDMS slabs with microchannels were compressed onto the MSNPs surfaces to form the UVS. G-UVS were fabricated by anodic bonding of PFS-modified glass microchannels and hydrophobic Si MSNP surfaces. In short, the glass microchannel and the Si surface were pressed together by the bonding machine (SUSS SB6e). In order to preserve the hydrophobic wettability of the chip surfaces, the heat time and temperature were set as 2 min and 350 °C, respectively, and it is worth noting that the chip should be quickly placed at a surface which could cool the chip after the bonding process. Repeated cleaning and modification of microchannel surfaces are required for successive dispensing of protein liquids and blood. We connected the UVS to a microfluidic flow control system (MFCS and FLOWELL, FLUIGENT) by a poly(tetrafluoroethylene) tube. The fluids in the UVS were pressure-driven, and the applied pressures of the inlets were controlled by the MFCS.

Synthesis of gold nanoparticles by the UVS. The synthesis of gold nanoparticles followed the well-established literature method, and the UVS was used for produced micro-quantitative nanoparticles. First, quantitative $HAuCl_4$ solutions (1 mM) blended with PVP solutions (180 mM) in the first mixed microchannels. Then, different quantities of ascorbic acid solutions (20 mM) were added to the mixed solutions. The solutions were transported to the second mixed microchannels by the pressure of the gas inlets. The second mixed microchannels should be set long enough and placed fishbone-shaped mixing structure to make sure the synthesis reaction is fully complete. Finally, the solutions containing the gold nanoparticles flowed to the position of copper meshes. The copper meshes were fixed in a deep reservoir under the outlet microchannels to insure that the gold nanoparticles solutions dripped onto the copper mesh totally. All the experiments were performed at 25°C, and the temperatures of the system were controlled by a thermoplate. The substrate surfaces and microchannels were modified with PFS to suppress reactor fouling.

Synthesis of gold nanorods by the UVS. The synthesis of gold nanorods followed the seed-growth method. The Au seeds were prepared by adding ice-cold sodium borohydride solution (0.5 mL of 0.015 mM) to a mixture of $HAuCl_4$ (5 mL of 1 mM) and CTAB (10 mL of 200 mM) solutions. Then, the mixture was stirred for 2 h, and freshly prepared seed particles were used for each experiment. The prepared process of the Au nanorods was performed in the UVSs, and the UVS-1 was used to capture quantitative liquids from the mixed solutions, including CTAB (4 mL of 250 mM), $HAuCl_4$ solution (4 mL of 1.25 mM) and silver nitrate solution (0.1 mL of 4 mM). The UVS-2 was used for capture quantitative ascorbic acid solutions (14.88 mM), and the UVS-3 was used for capture quantitative seed solutions. To obtain comparable volume of the quantitative additions in the UVSs, the original method was changed by diluting the reagent solutions (0.35 mL seed solution to 5 mL of water). All the experiments were performed at 29°C, and the temperatures of the system were controlled by a thermoplate. The substrate surfaces and microchannels were modified with PFS to suppress reactor fouling.

Characterization. Morphologies of the Si-MSNP structures were characterized by fluorescence microscopy (Olympus BX51 microscope), scanning electron microscope (JEOL FESEM 6700F) and atomic force microscopy

(AFM). Dimensions of the microchannels were measured by the Step Profiler (DEKTAK 150). Dataphysics OCA20 was performed to study the wetting properties of fluids on these surfaces and the ST of the fluids. The flow processes of fluids in the UVS were recorded by an Olympus fluorescence microscope. The volumes of the fluids were calculated based on the sizes of the narrow microchannels. TEM images were recorded using a H-800 electron microscope (Hitachi) at an acceleration voltage of 200 kV with a charged-coupled device camera. Data points in the figures are mean values of independent experiments. To meter the device-to-device variation, each point includes five same types of devices for more than 20 time cycle measurements, and the error bar was derived from measurement results.

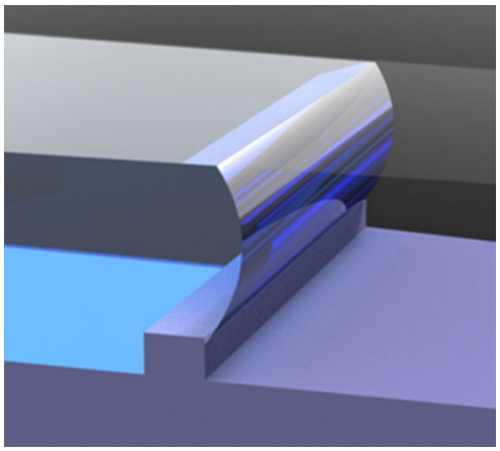

Figure S1. Schematic illustration of cambered fluid front at the right edge of the MSNP.

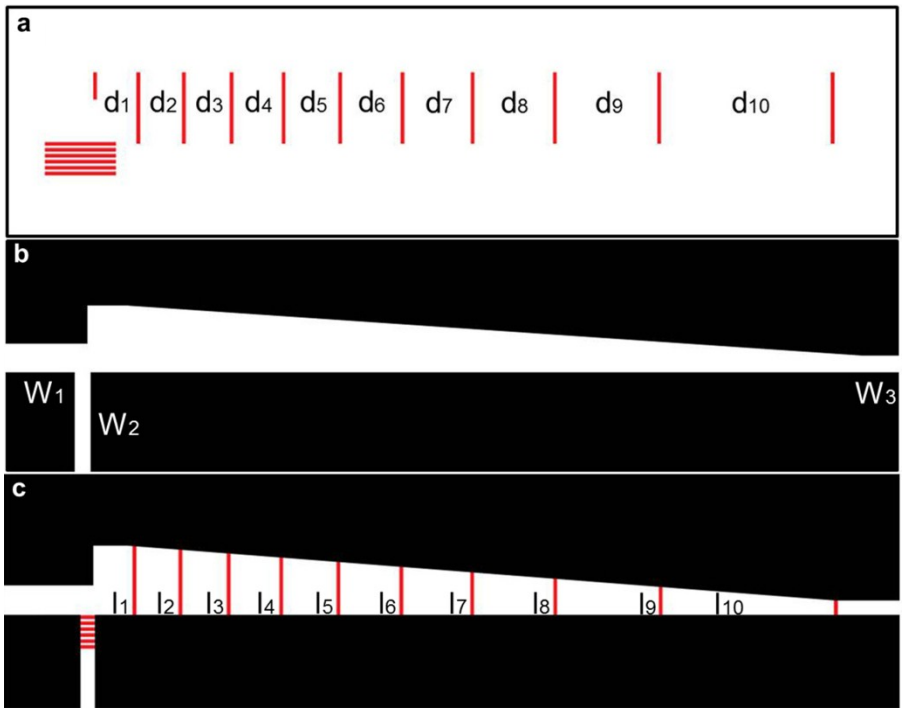

Figure S2. (a) Schematic of the MSNPs array, d represents the spacing of the MSNP centers. To reduce the distribution error when we capture the liquid by the gas, the volume of the first chamber is slightly more than one volume unit. (b) Schematic of the microchannel, W represents the widths of the microchannels. (c) Plane schematic of the UVS.

Table S1. The dimension parameters of the UVS/G-UVS.

Dimension [μm]	UVS 3 nL	UVS 2 nL	UVS 1 nL	UVS 0.5 nL	UVS 50 pL	G-UVS 6 pL	G-UVS 1.5 pL	G-UVS 500 fL	G-UVS 25 fL
d_1	260.0	260.0	260.0	260.0	81.0	31.0	19.3	14.8	8.6
d_2	256.1	256.1	256.1	256.1	80.9	30.7	19.0	14.6	
d_3	273.2	273.2	273.2	273.2	86.3	32.8	22.4	43.5	
d_4	292.8	292.8	292.8	292.8	92.5	35.1	28.8		
d_5	317.1	317.1	317.1	317.1	100.2	38.1	53.3		
d_6	348.8	348.8	348.8	348.8	110.2	41.9			
d_7	392.5	392.5	392.5	392.5	124.3	47.1			
d_8	457.9	457.9	457.9	457.9	144.7	55.0			
d_9	576.8	576.8	576.8	576.8	182.27	69.2			
d_{10}	914.8	914.8	914.8	914.8	289.1	109.8			
l_1	400.0	400.0	400.0	400.0	126.4	48.0	28.3	20.0	2.0
l_2	377.9	377.9	377.9	377.9	119.4	45.4	24.7	14.3	
l_3	354.4	354.4	354.4	354.4	112.0	42.5	20.3	3.1	
l_4	329.2	329.2	329.2	329.2	104.0	39.5	14.7		
l_5	301.8	301.8	301.8	301.8	95.4	36.2	4.3		
l_6	271.8	271.8	271.8	271.8	85.9	32.6			
l_7	238.0	238.0	238.0	238.0	75.2	28.6			
l_8	198.5	198.5	198.5	198.5	62.7	23.8			
l_9	148.8	148.8	148.8	148.8	47.0	17.9			
l_{10}	70.0	70.0	70.0	70.0	22.1	8.4			
W_1	250.0	250.0	250.0	250.0	60.0	24.0	15.0	10.0	
W_2	50.0	50.0	50.0	50.0	20.0	7.0	3.8	2.8	
W_3	70.0	70.0	70.0	70.0	22.1	8.4	4.3	3.1	
Channel height	30.0	20.0	10.0	5.0	4.8	4.2	3.0	2.0	1.5
MSNP width	10.0	10.0	10.0	10.0	2.0	1.5	1.5	1.5	1.5
MSNP height	1.5	1.5	1.5	1.5	1.0	0.5	0.3	0.2	0.1

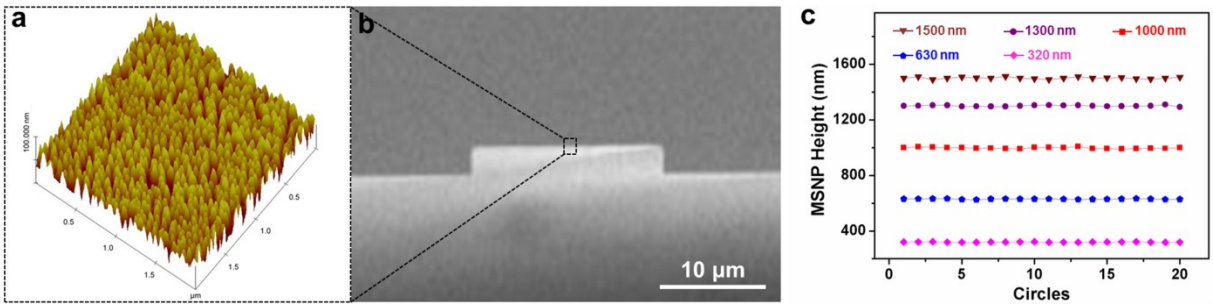

Figure S3. (a) AFM images of the nanopillars on the MSNP array surface. The etching time and roughness of the nanopillar are 35 s and 12.246±0.738 nm, respectively. (b) The SEM image of the MSNP. The height and width of the MSNP are 1500 nm and 10.0 μm, respectively. (c) Repeatability measures of the height of the MSNPs, and the accuracy rate are larger than 98.9%.

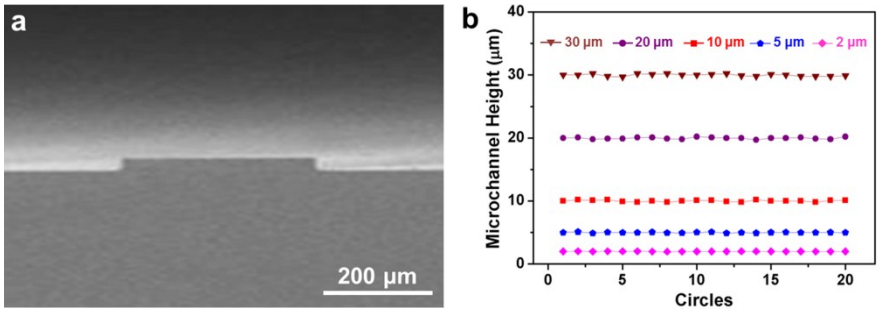

Figure S4. (a) The SEM image of the microchannel. The height and width of the microchannel are 10.0 μm and 200.0 μm, respectively. (b) Repeatability measures of the height of the microchannels, and the accuracy rates are larger than 99.0%.

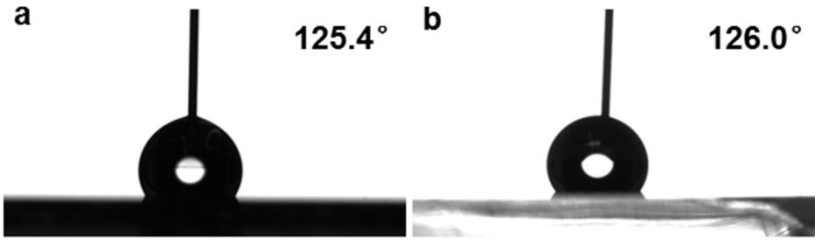

Figure S5. (a) The ACA of the PFS-modified Si MSNPs surface is 125.4±0.9°. (b) The ACA of the PDMS surface is 126.0±0.7°.

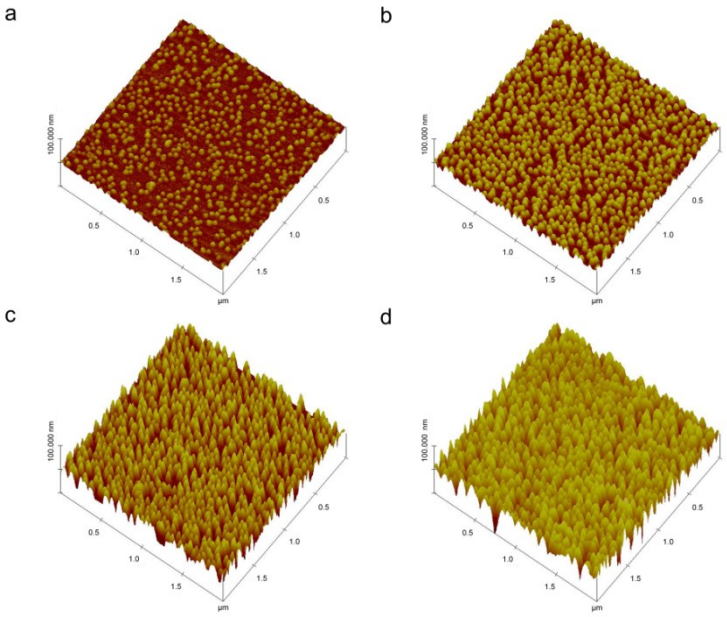

Figure S6. (a-d) AFM images of the nanopillars with different etching time on the MSNP array surface. The etching time and roughness of the nanopillar surfaces are (a) 5 s and 1.658±0.198 nm, (b) 15 s and 4.092±0.253 nm, (c) 25 s and 8.859±0.376 nm, (d) 45 s and 10.316±0.791 nm, respectively.

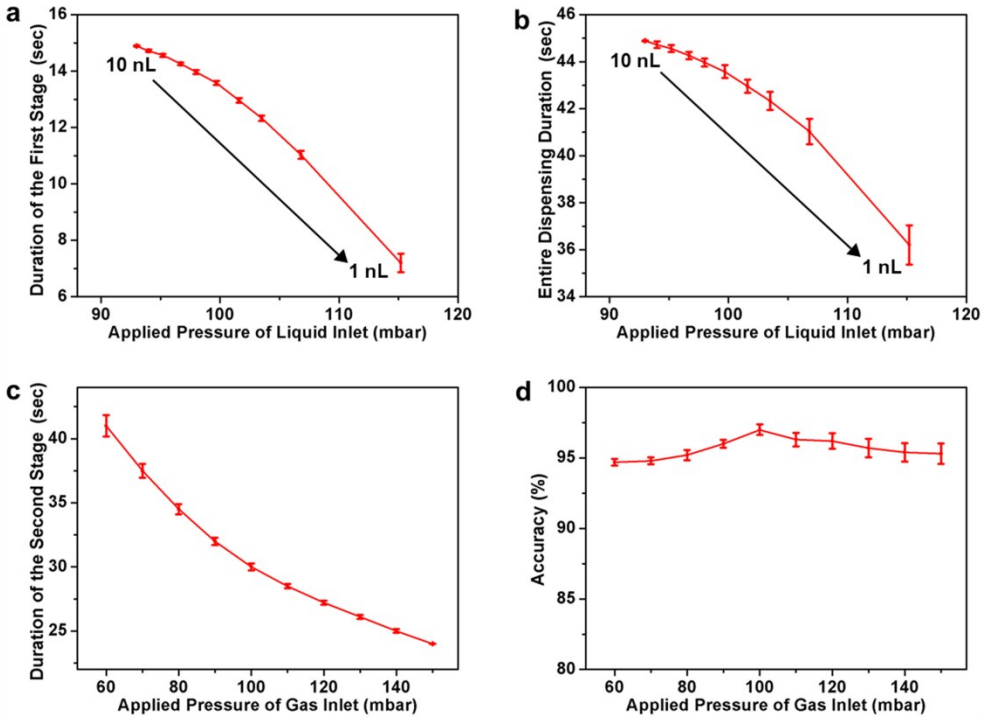

Figure S7. (a) The corresponding relationship between the liquid pressure and the duration of the first stage. (b) The corresponding relationship between the liquid pressure and the duration of the entire dispensing process when the gas pressure is 100.0 mbar. (c) The corresponding relationship between the gas pressure and the duration of the second stage. (d) The corresponding relationship between the gas pressure and the accuracy of the UVS.

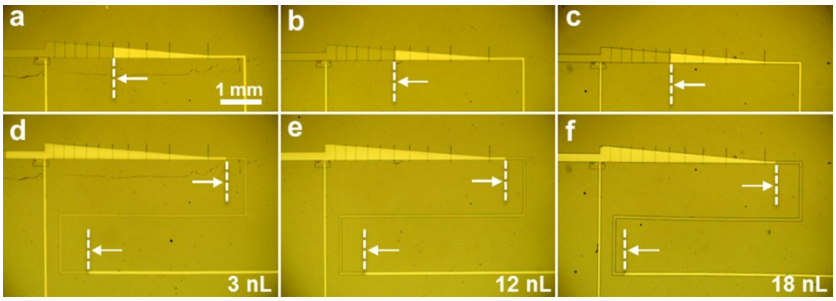

Figure S8. (a-f) Optical microscopy images of the UVSs with different measuring ranges. The microchannel heights of the UVS are 5.0 (a), 20.0 (b) and 30.0 μm (c), and the volume of each chamber is 0.5, 2.0 and 3.0 nL, respectively. 170.0, 56.0 and 37.0 mbar of the liquid inlet pressures are applied to stop the water fronts on the 6th MSNP in corresponding UVS. 120.0, 90.0 and 80.0 mbar of the gas inlet pressures are applied to obtain 3.07 (d), 12.18 (e) and 17.88 nL (f) water droplets, respectively. The figures in the images represent the desired liquid volumes.

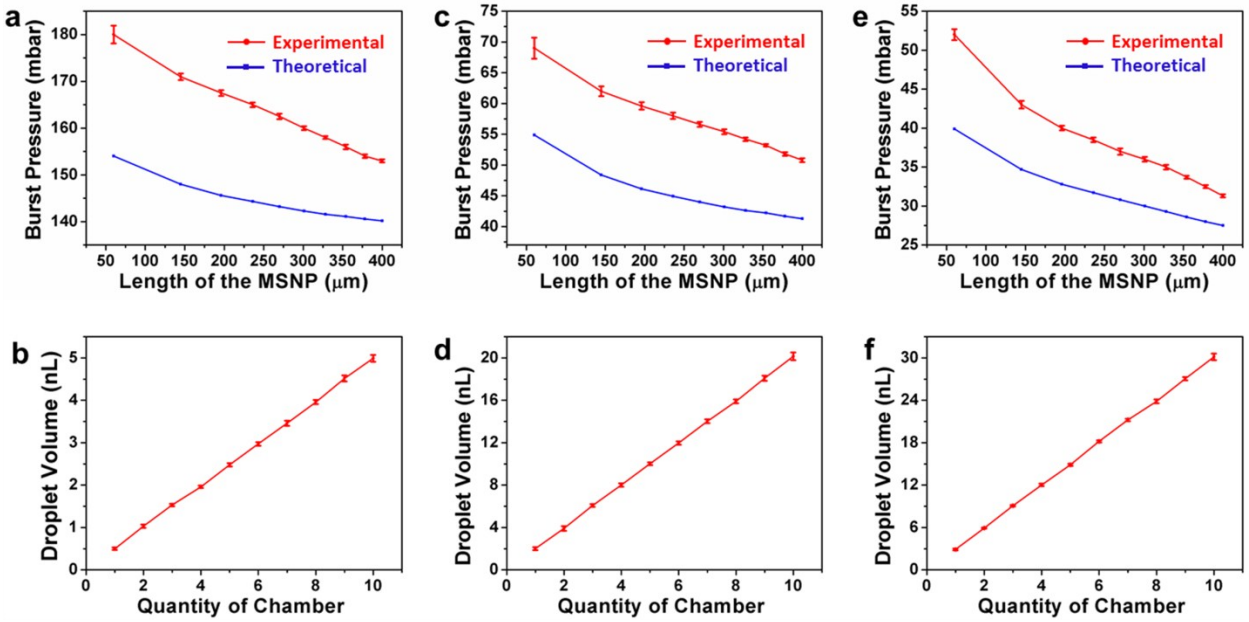

Figure S9. Experimentally measured and theoretical bursting pressures as a function of the length of exposed MSNPs in the microchannels, and the measured water volume dispensed as a function of chamber quantity. The ranges of the UVS are 5.00 (a, b), 20.00 (c ,d) and 30.00 nL (e, f), respectively. The accuracy rates of the three UVSs are larger than 97%. Errors bars represent standard error.

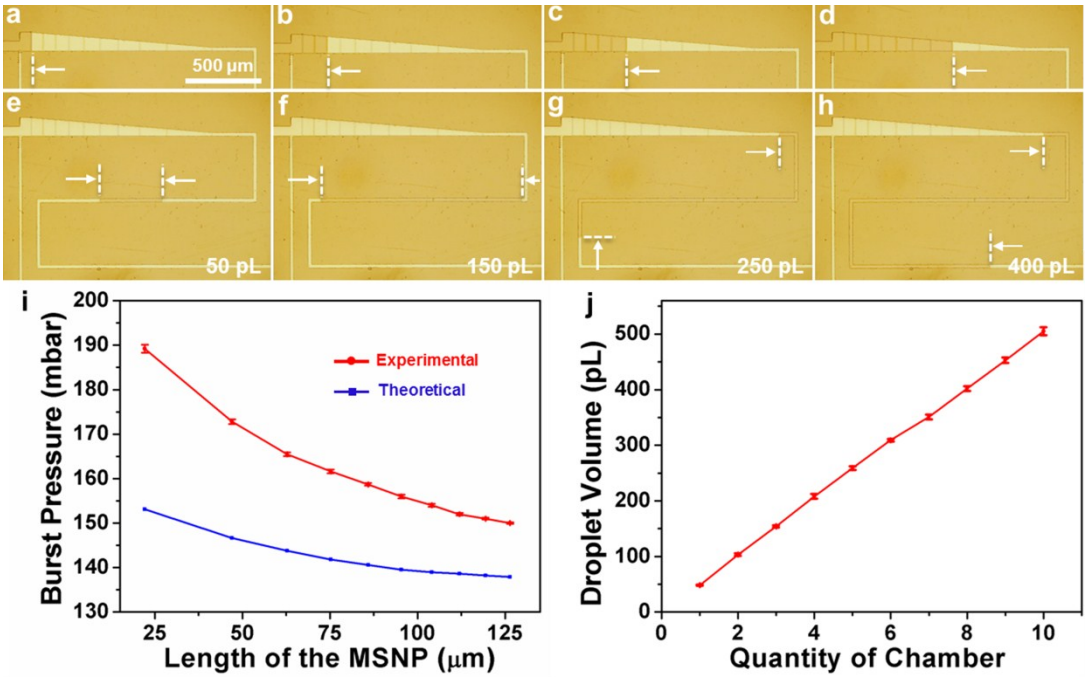

Figure S10. (a-d) Optical microscopy images of the dispensing process of water in the UVS. When the applied pressures of liquid inlets are 150.0, 152.0, 156.0 and 165.0 mbar, water front stop at the 1st (a), 3rd (b), 5th (c) and 8th (d) MSNP, respectively. The positions of white arrows represent the ends of the liquids. The height of the microchannel is 4.8 μm. The volume of each chamber is 50.0 pL theoretically. 0.0 mbar of liquid inlets and 200.0 mbar of gas inlets are applied to capture quantitative liquids in the UVS. The volumes of the water droplets are 48.8 (e), 151.8 (f), 256.0 (g), 400.4 pL (h), respectively. The figures in the images represent the desired liquid volumes. (i) Experimentally measured and theoretical bursting pressures as a function of the length of MSNPs in the UVS. (j) The measured water volume dispensed as a function of chamber quantity, and the accuracy rates of the UVS are larger than 96%. Errors bars represent standard error.

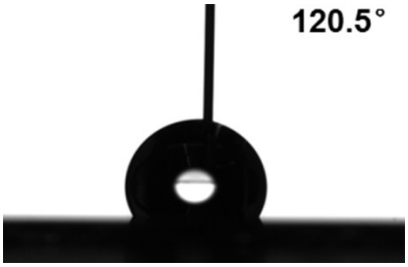

Figure S11. The ACA of the bonded PFS-modified Si MSNPs surface is 120.5±1.9°.

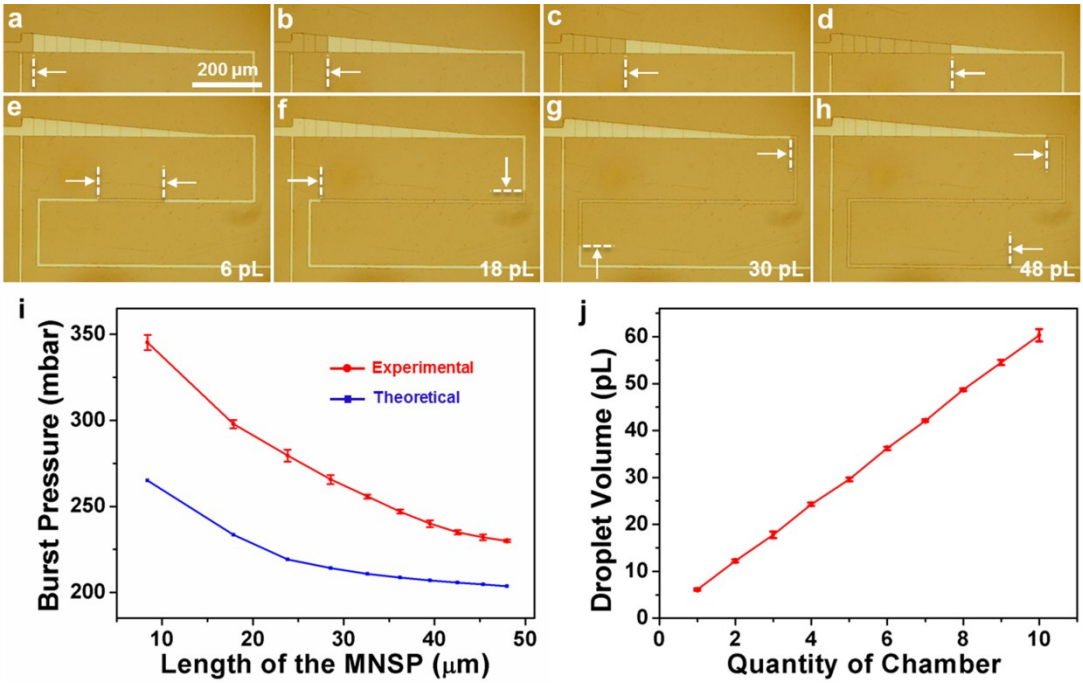

Figure S12. (a-d) Optical microscopy images of the dispensing process of water in the 10-G-UVS. When the applied pressures of liquid inlets are 230.0, 235.0, 247.0 and 280.0 mbar, water front stop at the 1st (a), 3rd (b), 5th (c) and 8th (d) MSNP, respectively. The positions of white arrows represent the ends of the liquids. The height of the microchannel is 4.2 μm. The volume of each chamber is 6.0 pL theoretically. 0.0 mbar of liquid inlets and 300.0 mbar of gas inlets are applied to capture quantitative liquids in the 10-G-UVS. The volumes of the water droplets are 6.0 (e), 18.5 (f), 30.3 (g), 47.5 pL (h), respectively. The figures in the images represent the desired liquid volumes. (i) Experimentally measured and theoretical bursting pressures as a function of the length of MSNPs in the 10-G-UVS. (j) The measured water volume dispensed as a function of chamber quantity, and the accuracy rates of the 10-G-UVS are larger than 97%. Errors bars represent standard error.

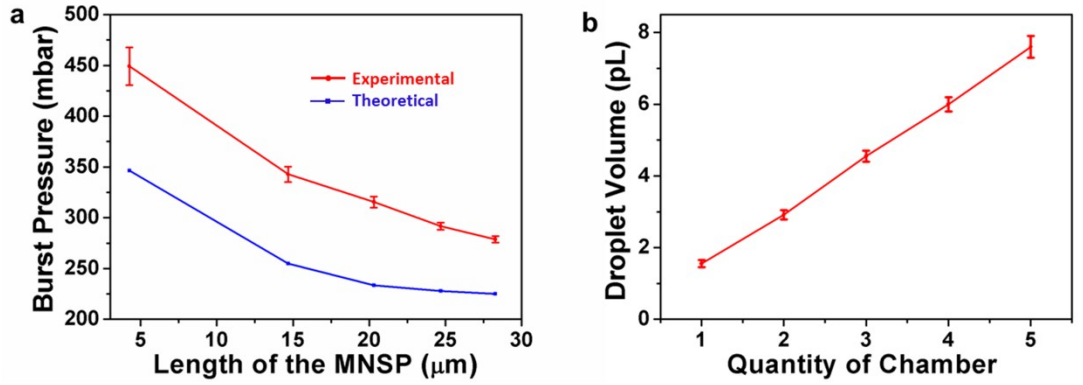

Figure S13. (a) Experimentally measured and theoretical bursting pressures as a function of the length of MSNPs in the 5-G-UVS. (b) The measured water volume dispensed as a function of chamber quantity, and the accuracy rates of the 5-G-UVS are larger than 96%. Errors bars represent standard error.

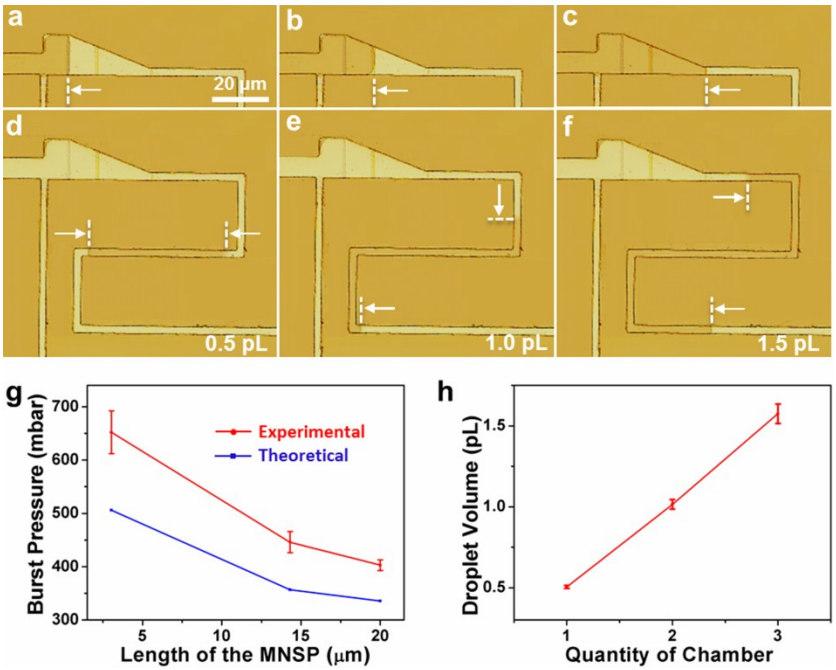

Figure S14. (a-f) Optical microscopy images of the dispensing process of water in the 3-G-UVS. When the applied pressures of liquid inlets are 403.0, 446.0 and 652.0 mbar, water front stop at the 1th (a), 2th (b) and 3th (c) MSNP, respectively. The positions of white arrows represent the ends of the liquids. The height of the microchannel is 3.0 μm. The volume of each chamber is 300 fL theoretically. 0.0 mbar of liquid inlets and 700.0 mbar of gas inlets are applied to capture quantitative liquids in the UVS. The volumes of the water droplets are 0.51 (d), 1.03 (e), 1.49 pL (f), respectively. The figures in the images represent the desired liquid volumes. (g) Experimentally measured and theoretical bursting pressures as a function of the length of MSNPs in the 3-G-UVS. (h) The measured water volume dispensed as a function of chamber quantity, and the accuracy rates of the 3-G-UVS are larger than 96%. Errors bars represent standard error.

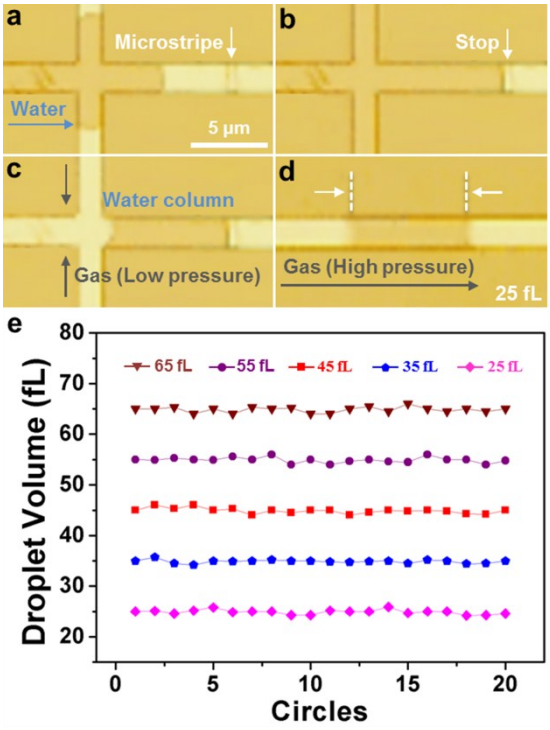

Figure 15. Optical microscopy images of the dispensing process of femtoliter liquid in the 1-G-UVS with fixed metering volume. (a) Water flows into the microchannel when the liquid pressure is 500.0 mbar. (b) Water front stops at the edge of the MSNP in the metering microchannel. (c) 600.0 mbar of the gas inlet pressures are applied to cut off the fluid column and captured quantitative water droplet. (d) 700.0 mbar of the three inlet pressures are applied to dispense 24.8-fL liquid. The figures in the images represent the desired liquid volumes. (e) Repeatability measures of the 1-G-UVS with different liquid volumes, and the accuracy rates of the device are larger than 97%. The circles represent the repeated measurement of the dispensing process.

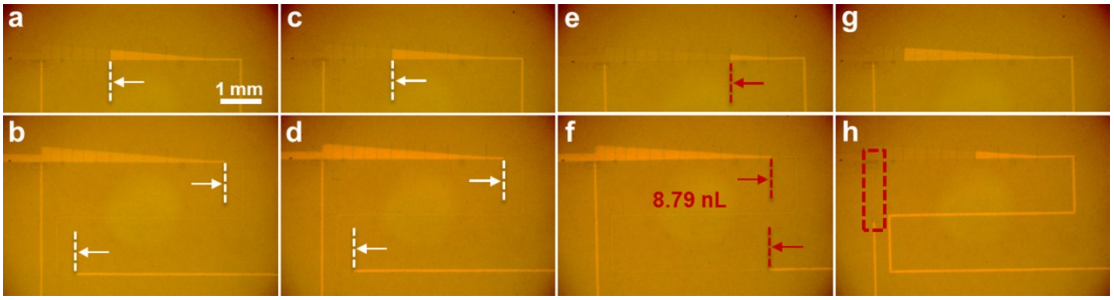

Figure S16. (a-h) Optical microscopy images of the UVS for capturing wide surface tension ranges liquids. The desired liquid volume is 6.00 nL. (a,b) 10% alcohol, ST is 48.23 mN/m, the manipulation pressures of liquid and gas inlets are 88.0 and 90.0 mbar. (c,d) 20% alcohol, ST is 40.6 mN/m, the manipulation pressures of liquid and gas inlets are 74.0 and 85.0 mbar. (e,f) 40% alcohol, ST is 28.2 mN/m. the manipulation pressures of liquid and gas inlets are 40.0 and 80.0 mbar. The UVS could not obtain quantitative desired liquid. (g,h) 50% alcohol, ST is 25.5 mN/m, the manipulation pressures of liquid and gas inlets are 30.0 and 80.0 mbar. The liquid flows to the gas inlet, and the UVS is no longer suitable.

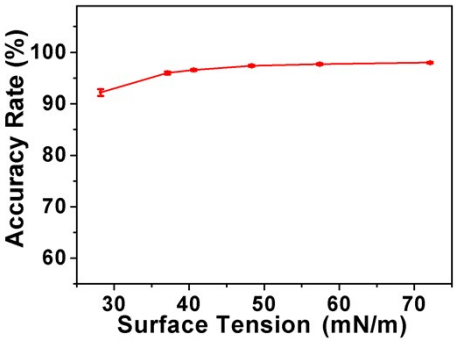

Figure S17. The corresponding relationship between the accuracy rate of the dispensing process and the ST of the captured liquids. Errors bars represent standard error.

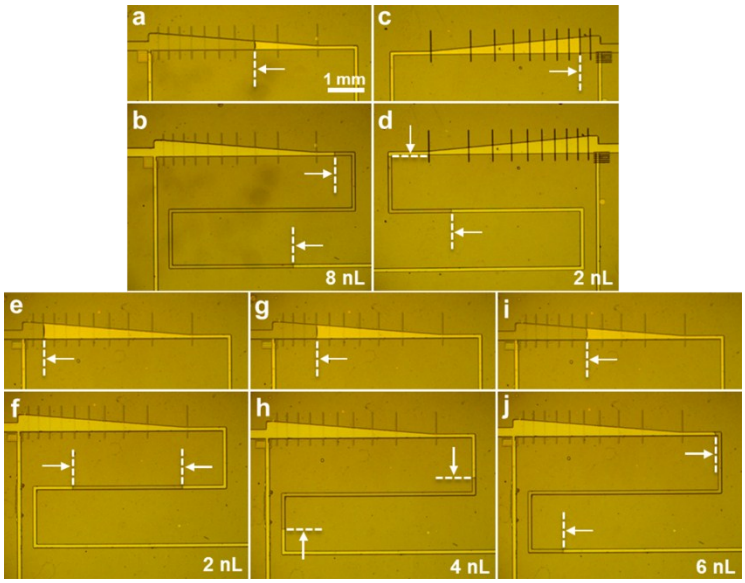

Figure S18. (a-j) Optical microscopy images of the UVS for capturing measurable solutions. The height of the microchannel is 10 μm. The figures in the images represent the desired liquid volumes. (a) 106.0 mbar of the liquid inlet is applied to stop the gold(III) chloride solution front on the right side of the 8th MSNP in the UVS-1. (b) 150.0 mbar of the gas inlet is applied to capture 7.97 nL gold(III) chloride solution. (c) 89.0 mbar of the liquid inlet is applied to stop the PVP solution front on the right side of the 2th MSNP in the UVS-2. (d) 150.0 mbar of the gas inlet is applied to capture 2.03 nL PVP solution. 89.0, 94.0 and 97.0 mbar of the liquid inlets are applied to stop the ascorbic acid solution fronts on the right side of the 2th (e), 4th (g) and 6th (i) MSNPs in the UVS-3, respectively. 150.0 mbar of the gas inlets are applied to capture 2.02 (f), 4.12 (h) and 6.00 (j) nL ascorbic acid solution.

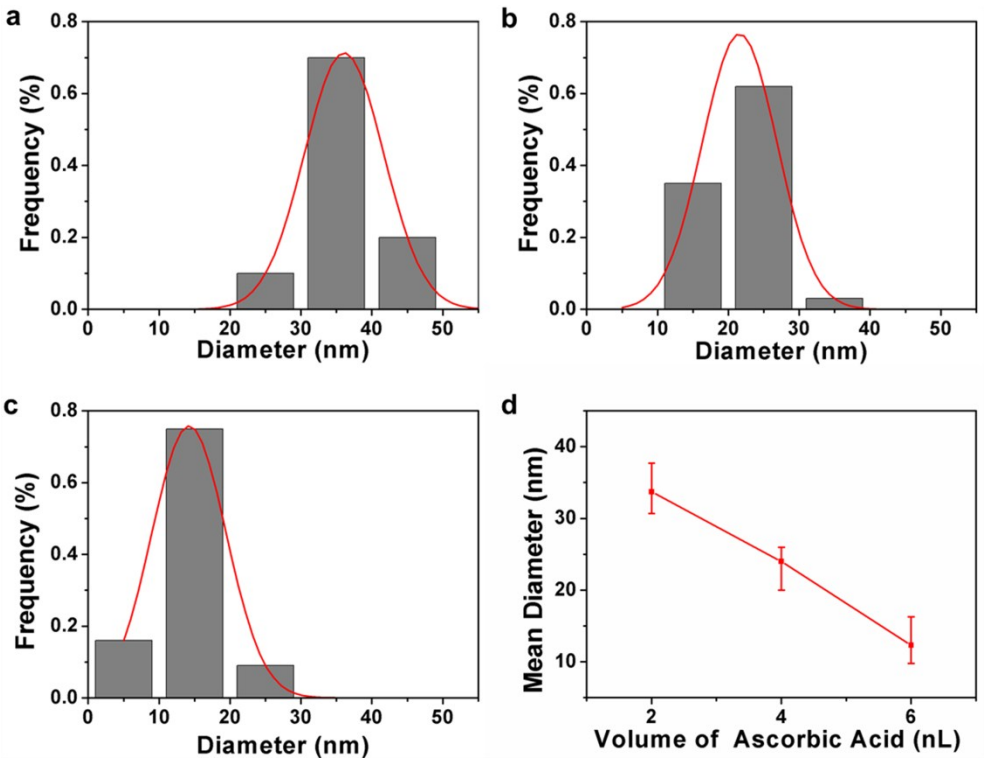

Figure S19. The diameter distribution of the Au nanoparticles, and the liquid volumes of the ascorbic acid solution are 2.02 (a), 4.12 (b) and 6.00 (c) nL. (d) The mean diameter of the Au nanoparticles as a function of the liquid volume of the ascorbic acid. Errors bars represent standard error.

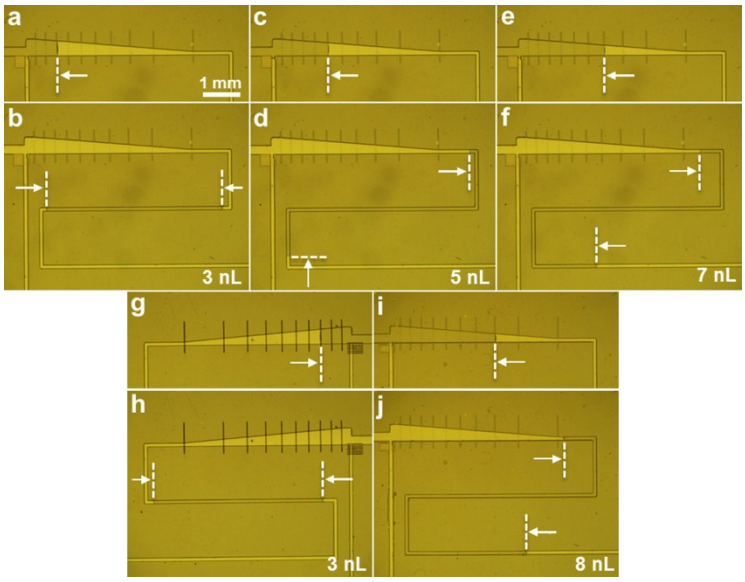

Figure S20. (a-j) Optical microscopy images of the UVS for capturing measurable solutions. The height of the microchannel is 10 μm. The figures in the images represent the desired liquid volumes. 75.0, 78.0 and 81.0 mbar of the liquid inlets are applied to stop the premixed solution ($Au^{[3+]}$, $Ag^{[+]}$, and CTAB solution) fronts on the right side of the 3rd (a), 5th (c) and 7th (e) MSNPs in the UVS-1, respectively. 150.0 mbar of the gas inlets are applied to capture 3.07 (b), 4.92 (d) and 7.05 (f) nL the premixed solutions. (g) 96.0 mbar of the liquid inlet is applied to stop the ascorbic acid solution front on the right side of the 3th MSNP in the UVS-2. (h) 150.0 mbar of the gas inlet is applied to capture 3.02 nL ascorbic acid solution. (i) 104.0 mbar of the liquid inlet is applied to stop the Au seed solution front on the right side of the 8th MSNP in the UVS-3. (d) 150.0 mbar of the gas inlet is applied to capture 7.99 nL Au seed solution.

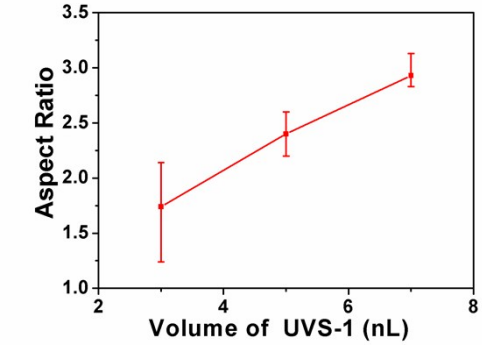

Figure S21. The mean aspect ratio of the Au nanorods as a function of the liquid volume of the premixed solution ($Au^{[3+]}$, $Ag^{[+]}$, and CTAB solution). Errors bars represent standard error.